Ventilation Changes Drive Orbital-Scale Deoxygenation Trends in the Late Cretaceous Ocean

Anta Clarisse Sarr, Yannick Donnadieu, Marie Laugié, Jean Baptiste Ladant, Baptiste Suchéras-Marx, François Raisson

AGU ADVANCING EARTH AND SPACE SCIENCE

Geophysical Research Letters®

RESEARCH LETTER
10.1029/2022GL099830

Ventilation Changes Drive Orbital-Scale Deoxygenation Trends in the Late Cretaceous Ocean

A.-C. Sarr[1], Y. Donnadieu[1], M. Laugié[1], J.-B. Ladant[2], B. Suchéras-Marx[1], and F. Raisson[3]

[1]Aix Marseille University, CNRS, IRD, INRAE, College of France, CEREGE, Aix-en-Provence, France, [2]Laboratoire des Sciences Du Climat et de l'Environnement, LSCE/IPSL, CEA-CNRS-UVSQ, Université Paris-Saclay, Gif-sur-Yvette, France, [3]TotalEnergies, Pau, France

Key Points:

- Small orbitally induced changes in ventilation produce large-scale modification of O_2 distribution in the late Cretaceous ocean
- Deoxygenation is strongly enhanced in already poorly oxygenated basins such as the proto-Atlantic ocean
- Variations in deoxygenation strength occurs at all orbital frequency albeit with different amplitude

Supporting Information:

Supporting Information may be found in the online version of this article.

Correspondence to:

A.-C. Sarr,
anta.clarisse.sarr@gmail.com

Citation:

Sarr, A.-C., Donnadieu, Y., Laugié, M., Ladant, J.-B., Suchéras-Marx, B., & Raisson, F. (2022). Ventilation changes drive orbital-scale deoxygenation trends in the late Cretaceous ocean. *Geophysical Research Letters*, *49*, e2022GL099830. https://doi.org/10.1029/2022GL099830

Received 14 JUN 2022
Accepted 20 SEP 2022

Author Contributions:

Conceptualization: A.-C. Sarr
Formal analysis: A.-C. Sarr
Funding acquisition: Y. Donnadieu, F. Raisson
Investigation: A.-C. Sarr, M. Laugié
Methodology: A.-C. Sarr, M. Laugié, J.-B. Ladant
Supervision: Y. Donnadieu
Visualization: A.-C. Sarr
Writing – original draft: A.-C. Sarr
Writing – review & editing: A.-C. Sarr, Y. Donnadieu, M. Laugié, J.-B. Ladant, B. Suchéras-Marx, F. Raisson

Abstract Mechanisms that drive cyclicity in marine sediment deposits during hothouse climate periods in response to Earth's orbit variations remain debated. Orbital cycles fingerprint in the oceanographic records results from the combined effect of terrestrial (e.g., Weathering derived nutrient supply, freshwater discharge) and oceanic (e.g., productivity, oxygenation) processes, whose respective contribution remains to be clarified. Here we investigate the effect of extreme orbital configurations on the oxygenation state of the ocean using marine biogeochemistry simulations with the IPSL-CM5A2 Earth System Model under Cenomanian-Turonian boundary conditions. Our simulations show that small changes in ocean ventilation triggered by orbitally induced variations in deep water formation have a strong impact on the spatial distribution of dissolved oxygen. This phenomena is amplified in enclosed and already poorly oxygenated basins, such as the proto-Atlantic ocean, where up to 50% of the water volume become anoxic for some of the configurations.

Plain Language Summary Changes in the orbit of the Earth over time are responsible for periodic perturbations of the atmosphere and ocean dynamics that are ultimately being recorded in marine sediments through the occurrence of cyclicity. Origin of these cycles in past sedimentary records is not well understood because they are the result of the interactions between different processes that all exert a control on the nature of the deposited sediments. One of these processes is the oxygenation of the ocean that controls the potential for preservation of deposited organic matter. Here we focus on how variations in ocean dynamics modulate the oxygenation of the ocean during the late Cretaceous, using paleoclimate model simulations. We find that small changes in the oceanic circulation can lead to strong loss in oxygen in some part of the ocean, such as the Central Atlantic. Our results have implication for understanding the sedimentary record, the functioning of biogeochemical cycles and feedbacks within the climate system.

1. Introduction

By modulating the amount and distribution of solar radiations received at the surface of the Earth, changes in Earth's orbit and rotational axis generate significant periodic perturbations in the climate system. Those perturbations remain imprinted in the sedimentary record in the form of high frequency cyclicity in sedimentation (e.g., Einsele, 1982; Rossignol-Strick, 1985; Westerhold et al., 2020), which is generally reflected in the alternation of limestone and marl lithologies. Rhythmic sedimentation paced by orbital variation is especially well documented in the Cretaceous sedimentary record from the Atlantic and Tethyan margins (e.g., Barron et al., 1985; Batenburg et al., 2016; Beckmann et al., 2005; Beil et al., 2018; Charbonnier et al., 2018; Dickson et al., 2017; Eldrett et al., 2015; Hofmann & Wagner, 2011; Kolonic et al., 2005; Kuhnt et al., 2017; Kuypers et al., 2004; Li et al., 2020; Mitchell et al., 2008; Sageman et al., 1997; van Helmond et al., 2015; Voigt et al., 2008; Wang et al., 2022). In part of those records dating from Ocean Anoxic Events (OAEs)—that represent periods of carbon cycle perturbation under extreme greenhouse configuration —the cyclicity is characterized by the alternation of black shales and organic-poor sediments (Herbert & Fischer, 1986; Kuhnt et al., 2017; Kuypers et al., 2004; van Helmond et al., 2015). Cycles are also evidenced by variations in organic matter (OM) quality and/or origin (continental vs. marine) (e.g., Dummann et al., 2021), or in carbonate content or $\delta^{13}C$ signature (Kuhnt et al., 2017), depending on the oceanographic setting and site location.

Unraveling the mechanisms involved in cyclic OM deposition is important to understand the functioning of biogeochemical cycles and feedbacks within the climate system; and the existence of such cyclicity in ocean sediment records from extreme greenhouse periods questions the mechanisms at play as cycles cannot be

Table 1
Orbital Parameters Values for the Simulations

Simulation	Eccentricity	Precession[a]	Obliquity
LO	0	–	22.1
HO *(ref)*	0	–	24.5
HOWP	0.06	90	24.5
HOSP	0.06	270	24.5
HOAP	0.06	0	24.5
HOVP	0.06	180	24.5

Note. Eccentricity, obliquity and precession respectively describe the shape of Earth orbit, the tilt of Earth rotational axis and the timing with respect to the Northern Hemisphere seasons of Earth's closest proximity to the sun; and control the latitudinal and seasonal distribution of insolation (Figure S3 in Supporting Information S1). HO and LO have a circular orbit and therefore no perihelion. HO serves here as a reference simulation.

[a]longitude of the perihelion (ω).

explained by the non-linearities related to ice-sheets dynamics in contrast to late Cenozoic and Quaternary periods. Organic-rich layers of sediments are often associated with indicators of enhanced continental inputs (pollens abundance, chemical elements indicative of enhanced weathering, detrital sediments) (e.g., Batenburg et al., 2016; Beckmann et al., 2005; Charbonnier et al., 2018; Dummann et al., 2021; van Helmond et al., 2015) and/or increased surface-ocean stratification (van Helmond et al., 2015), as well as indicators of changes in seafloor redox conditions (Dummann et al., 2021; Hofmann & Wagner, 2011; Kolonic et al., 2005). Orbital variations in OM deposits are therefore often interpreted as the result of periodic enhancement of continental river discharge combined with enhanced weathering via eccentricity-modulated fluctuation of the Inter-Tropical Convergence Zone position. The input of nutrients to the ocean would have increased consequently and would have stimulated primary productivity (e.g., Beckmann et al., 2005; Wagner et al., 2013). Combined with increasing upper ocean stratification, this would also have locally stimulated anoxia (e.g., Beckmann et al., 2005; Behrooz et al., 2018; Flögel et al., 2008) and therefore potential for OM preservation; both processes contributing to periodic formation of organic-rich layers. Alternatively, Meyers et al. (2012) suggest that the cyclic variations recorded in the sediments of Central Atlantic basins reflect variations of intermediate to deep water formation that affect oxygen availability (ventilation cycles) and therefore OM preservation potential at the seafloor. In this study, obliquity has been identified as a principal pacemaker of OM variations and because obliquity largely influence climate of high latitudes, Meyers et al. (2012) hypothesis that the signal have been impulsed from deep/intermediate water formation areas at high latitude.

Mechanisms that drive changes in the ocean-atmosphere dynamics under variable orbital configurations have previously been analyzed using dedicated paleoclimate simulations for greenhouse climate periods (Beckmann et al., 2005; Dummann et al., 2021; Floegel & Wagner, 2006; Flögel et al., 2008; Park & Oglesby, 1991; Sloan & Huber, 2001; Winguth & Winguth, 2013). Most of these modeling studies have tentatively linked changes in the hydrological cycle to the cyclicity of OM deposits via orbitally driven modulation of freshwater discharge and nutrient fluxes (Beckmann et al., 2005; Dummann et al., 2021; Floegel & Wagner, 2006; Flögel et al., 2008). However, these studies have neglected the effect of ocean dynamics on both oxygen distribution and biological production, leaving a missing piece to decipher the role of oxygenation on the signal via preservation potential for OM. As a first step toward filling this gap, we here investigate the impact of orbital parameter changes on global oxygenation trends during the Cenomanian-Turonian.

2. Method

We performed fully coupled simulations with the IPSL-CM5A2 Earth System Model (Sepulchre et al., 2020) supplemented with extensions using only its marine biogeochemical module PISCES-v2 (Aumont et al., 2015). Both have been previously used to simulate Cenomano-Turonian climate and paleoceanography (Laugié et al., 2020, 2021). Simulations have been performed with a paleogeographic reconstruction for the Cenomanian-Turonian (Figure S1 in Supporting Information S1) that combined the land-sea configuration of Sewall et al. (2007) with the bathymetry from Müller et al. (2008). Atmospheric pCO_2 has been prescribed to four times the pre-industrial value (1,120 ppm). Previous analyses demonstrated that these characteristics provide a realistic simulation of the Cenomanian-Turonian climate with the IPSL-CM5A2 model (Laugié et al., 2020). Detailed information about models, simulations setup and equilibrium can be found in Supporting Information S1 (Texts S1 and S2 and Figure S2 in Supporting Information S1). We used a set of six idealized orbital simulations (Table 1) in order to test the sensitivity of the ocean-atmosphere system to orbital changes (see Supporting Information S1 for detailed protocol). Because the numerical solution for orbital parameters become highly uncertain for periods before 50 Ma (Laskar et al., 2011), we used end-member configurations with extreme eccentricity, obliquity, and precession values instead of varying the three parameters together. Those configurations enable us to isolate and analyze the effects of each parameter on the climate system (e.g., Erb et al., 2015). LO and HO experiments represent obliquity extremes, with an axial tilt of 22.1° and 24.5° respectively and an eccentricity set to zero, rendering the Earth's orbit round and nullifying the impact of precession. In HO, the insolation is maximized at

high latitudes during summer in both hemispheres and slightly increased in the tropics and mid-latitudes during winter, which decreases the meridional gradient of temperature compared to LO (Figure S3 in Supporting Information S1). The HOAP, HOWP, HOVP, and HOSP experiments are used to explore the effect of eccentricity and precession, considering different longitude of the perihelion from the moving equinox (Laskar et al., 2004) (0, 90, 180, and 270° respectively). In this set of simulations, eccentricity is set to 0.06, close to its maximum value, so the effect of precession is maximized. Precession modulates the seasonal cycle of insolation and determines the season of increased insolation (Figure S3 in Supporting Information S1): insolation is enhanced in the Northern Hemisphere during boreal summer, when the perihelion is on the 21st of June (HOSP) (Figure S3 in Supporting Information S1). HOSP and HOVP configurations maximize the insolation during tropical wet season (spring and summer), which results in increased seasonality within the tropics with the strengthening of monsoonal precipitations.

As we here focus on oxygenation changes related to modifications in ocean circulation, we impose the total global annual amount of nutrient in each of the PISCES simulations with different orbital configurations to equal the preindustrial amount (see Supporting Information S1 for additional details). This means that the spatial distribution of dissolved nutrient concentrations depends only on the ocean circulation and intensity of freshwater discharge and that modifications in the global supply of nutrients related to changes in weathering intensity are not considered.

3. Results

3.1. Orbitally Induced Deoxygenation Trends

In our simulations, most of the ocean and ocean seafloor remain oxic with exception of the Atlantic basin (Figure 1a and Figures S4 and S5 in Supporting Information S1), such as already described by Laugié et al. (2021). Strong oxygenation is simulated from the seafloor to the subsurface in the southern Pacific ocean (>250 mmol/m^3) as well as in the Arctic basin, while intermediate O_2 concentrations (80–120 mmol/m^3) are depicted in the Eastern Equatorial Pacific, on bathymetric highs in the Pacific ocean and Kerguelen Plateau as well as in the deepest part of the European Tethys (Figure 1a). In the Atlantic ocean more than 70% of the water volume is below the limit for dysoxia and most of the seafloor is anoxic (<6.5 mmol/m^3) or dysoxic (<62.5 mmol/m^3) in all the configurations (Figure 1 and Figure S4 in Supporting Information S1). Within this basin, orbitally forced trends in deoxygenation are dominated by the oxygenation state of the Central Atlantic basin (CA), whose seafloor is permanently below the oxygen concentration threshold for dysoxia (Figure 1a and Figure S4 in Supporting Information S1). At the seafloor, the eastern part of the Central Atlantic becomes anoxic for some orbital configurations, whereas the western part, that encompasses the Gulf of Mexico, remains dysoxic despite losing oxygen (Figure 1a and Figure S4 in Supporting Information S1). The volume of anoxic waters in the Central Atlantic consequently varies from less than 10% to up than 55% of the global volume between the two end-members simulations (HO and HOVP) (Figure 1b). Obliquity extremes generate a doubling in the volume of anoxic water (from 10 (HO) to 20% (LO)), while precession changes (in maximum eccentricity configuration) yield expansion of anoxia from 25% to 50% of the basin volume (HOAP vs. HOVP). This highlights a strong effect of eccentricity on the oxygenation state of the Central Atlantic ocean. In the central Atlantic region, the seafloor is permanently anoxic in the equatorial Atlantic gateway region and turns to a dysoxic state in the southern part, north of the Walvis ridge (EA) (Figure 1a and Figure S4 in Supporting Information S1). South of the Walvis ridge (SWR region on Figure 1), the seafloor is close to the dysoxia threshold but remains mostly oxic in the zero-eccentricity experiments (>90% of the water mass is above the threshold; Figure 1b—LO and HO). The seafloor however never reaches an anoxic state and continental platforms on both sides of the basin remain well oxygenated. In HOSP configuration, dysoxic waters at the seafloor extends to the austral part of the Atlantic region (Figure 1a and Figure S4 in Supporting Information S1). The volume of oxygenated waters in the South Atlantic decreases with increasing eccentricity as dysoxia extends south of the Walvis ridge periodically within a precession cycle and can reach up to 50% of the basin volume in the HOSP and HOVP configurations (Figure 1b).

Oxygen depletion mostly occurs at intermediate and deep water depth: a strong vertical oxygen gradient is seen in the Central Atlantic basin with a large amplification of oxygen loss below the Oxygen Minimum Zone (OMZ) (below 600 m) (Figure S6 in Supporting Information S1). The global deoxygenation pattern is similar for each of the configurations relative to HO, though with subtle differences in the intensity and geographic pattern. Decrease

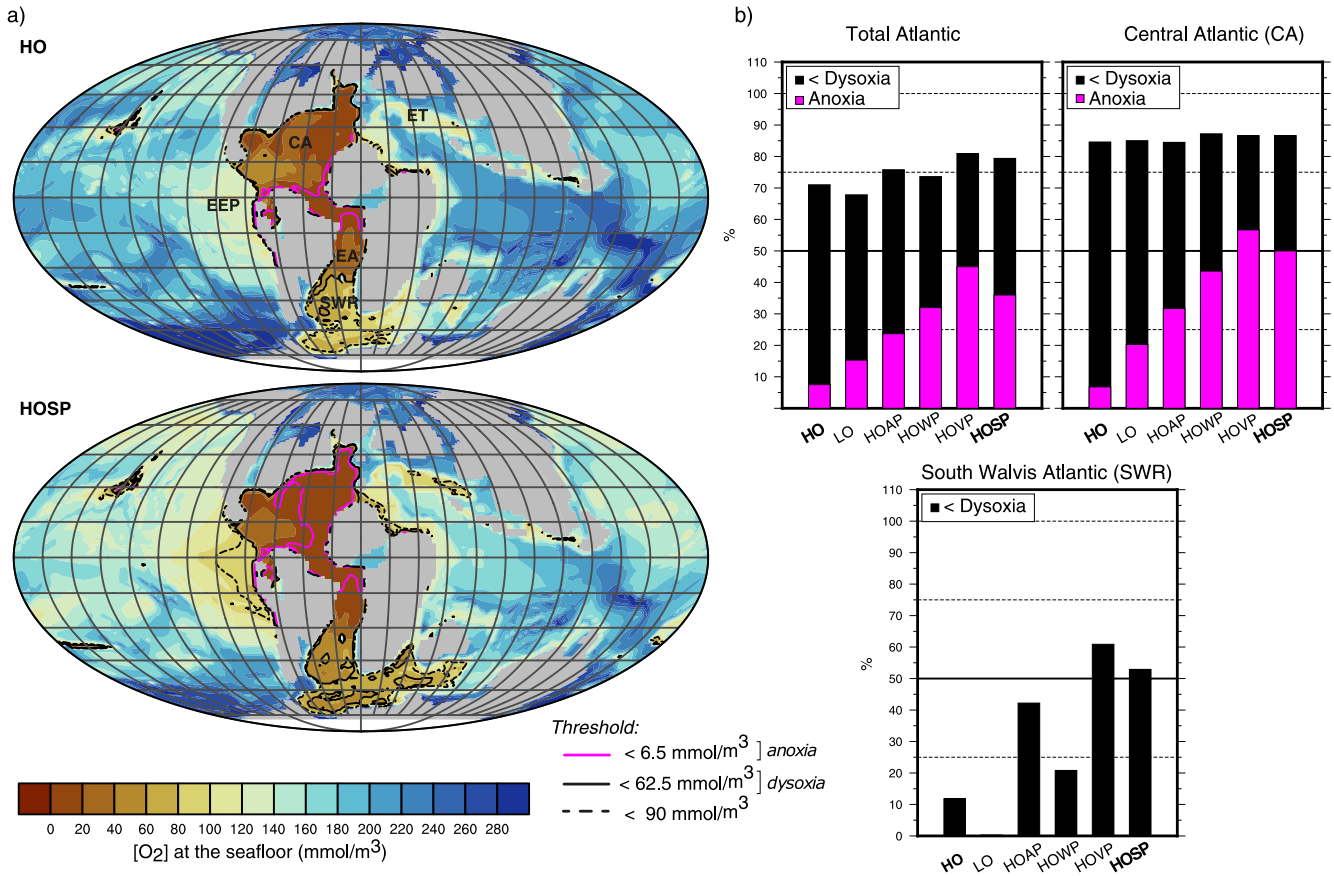

Figure 1. (a) Dissolved O_2 at the seafloor for HO (left) and HOSP (right). Lines show the limit of dysoxic and anoxic waters respective to the tresholds we used for this study. Here we set up the threshold for anoxia at the O_2 value below which denitrification initiate in the model (6.5 mmol/m^3, magenta line). Threshold for dysoxia is setup at 62.5 mmol/m^3 following Middelburg and Levin (2009) (thick black line) to keep consistency with Laugié et al. (2021), although the value of mmol/m^3 is also find in literature (Tyson & Pearson, 1991) (dashed black line). (b) Percentage of ocean volume below anoxia and dysoxia thresholds in the Atlantic region, Left: Atlantic Basin; Middle: Northern Atlantic Basin; Right: Southern Atlantic basin (south of the Walvis Ridge). Values represent averages over the last 100 years of the simulations. CA—Central Atlantic, EA—Equatorial Atlantic, SWR—South Atlantic, south of Walvis rigde, ET—European Tethys platforms, EEP—East Equatorial Pacific.

in O_2 content at intermediate depth and at the seafloor is also simulated in the southern Atlantic basin for the most deoxygenated configurations (HOSP and HOVP) (Figure S6 in Supporting Information S1 and Figure 1b).

3.2. Ventilation Control on O_2-Depletion

In the following we focus on the HO and HOSP configurations that present strong contrast in oxygenation states (Figure 1b) in order to analyze the forcing mechanisms of O_2 variations. Variations in O_2 content is function of (a) O_2 saturation (O_2Sat), that represents the maximum amount of O_2 a water mass can hold at given temperature and salinity and (b) the AOU that corresponds to the balance between ventilation and remineralization processes related to biological activity. O_2 content of the water mass equals O_2sat minus AOU (Bopp et al., 2017). Simulated O_2 trends are largely superimposed with changes in AOU (Figures 2a–2c and 2f–2h). In the Atlantic basin for example, subsurface (200–600 m) changes in AOU drives more than 80% of the total subsurface change in O_2 content, highlighting the prime effect of ventilation/remineralization processes over the thermal one in the simulated signal. In the deep ocean, the contribution of O_2Sat to O_2 changes is negligible (Figure 2g).

Increase in AOU can be driven either by enhanced biological O_2 consumption from remineralization processes due to increased biological activity, or by a decrease in ventilation or an increase in water stratification (Bopp et al., 2017). No obvious relationship exists between changes in subsurface AOU and changes in patterns of export productivity at global scale between the HOSP and HO configurations (Figures 2c and 2e). In regions such as the northern Atlantic basin and the North Pacific Ocean, export productivity and O_2 concentration even

10.1029/2022GL099830

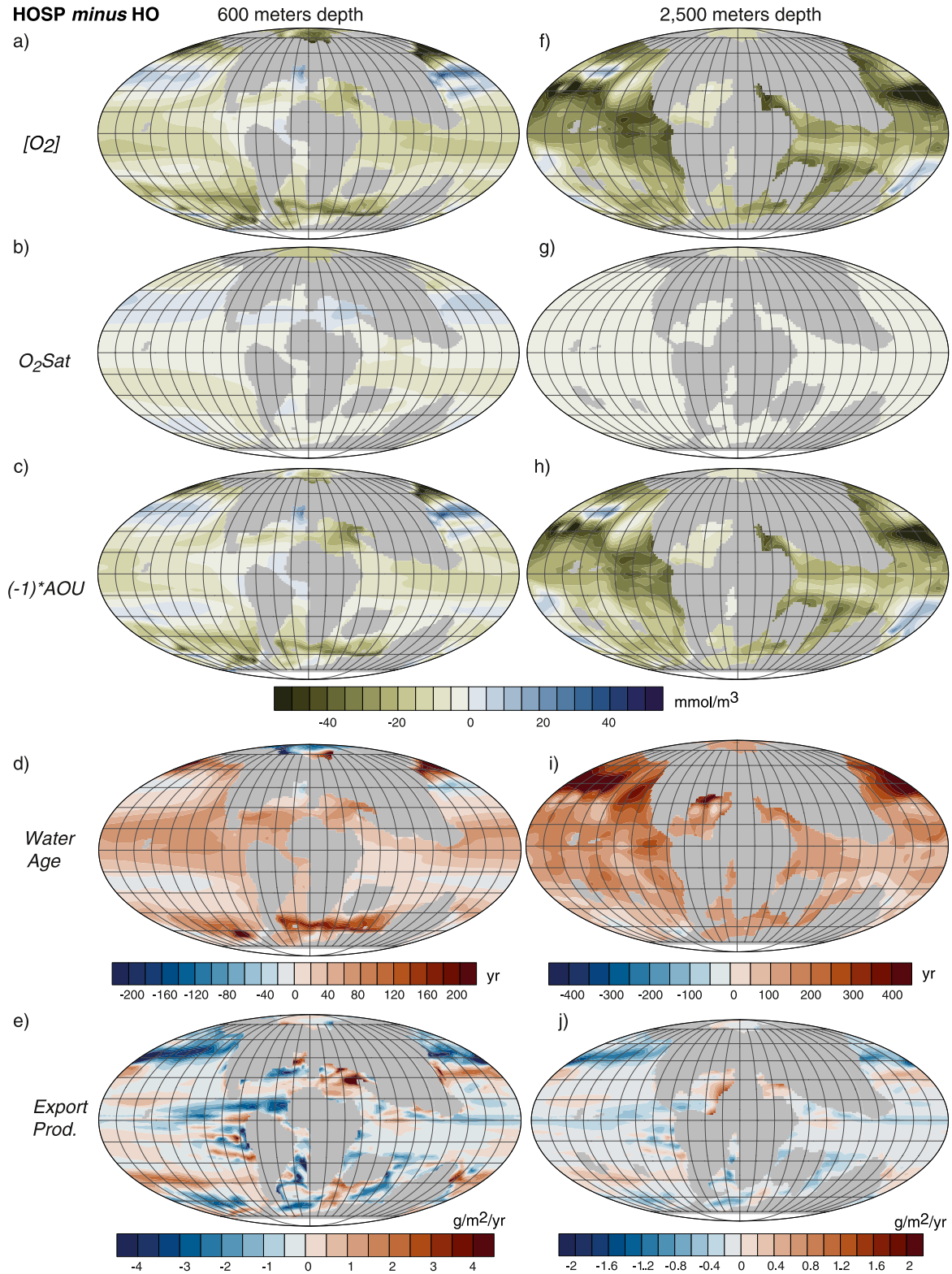

Figure 2. Change in (a–f) O_2 concentration; (b–g) O_2 saturation (O_2Sat); (c–h) Apparent Oxygen Utilisation ((-1)*AOU); (d–i) Water mass age and (e–j) Export Production, between HOSP and HO configurations. Left: at 600 m depth; Right, at 2,500 m depth (below the OMZ). $O_2 = O_2\text{Sat}—[\text{AOU}]$.

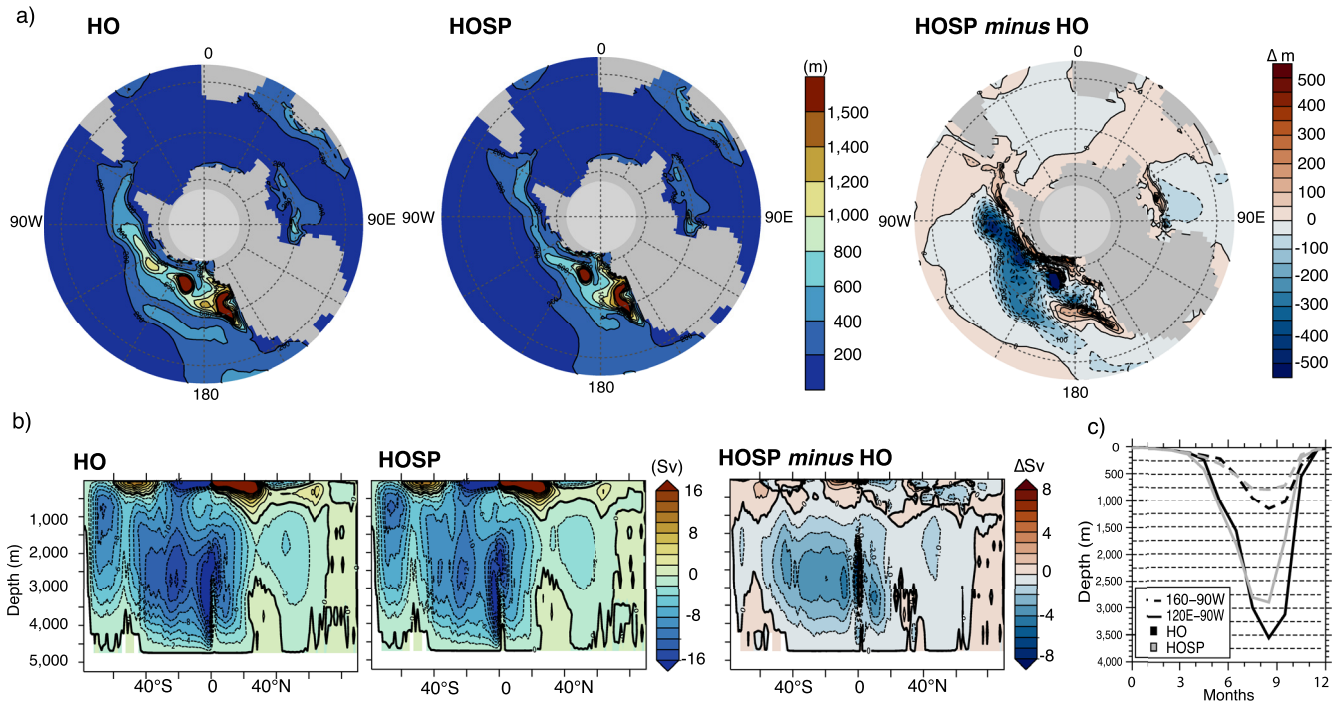

Figure 3. (a) Winter maximum mixed layer depth in HO (left) and HOSP (middle) and difference in Winter maximum mixed layer depth (HOSP minus HO; right). (b) Meridional Overturning Circulation (Sv) in the HO (left) and HOSP (middle) configuration and difference between HOSP and HO (right). Absolute values have been taken to compute the difference so negative values shows decreasing intensity of the circulation. (c) Monthly variation of the maximum depth of the mixed layer along the Antarctica margin in the Pacific Ocean (80°S-60°S), where part of the deep and deep intermediate water masses form.

decrease simultaneously in HOSP relative to HO (Figures 2e and 2j). In addition, deoxygenation mostly occurs below the OMZ (Figure S6a in Supporting Information S1), suggesting a strong control by ventilation. This is confirmed by the ideal age of water masses, a tracer commonly used to track changes in ventilation (e.g., Bopp et al., 2017; Ladant et al., 2020), the pattern change of which correlates with changes in AOU patterns (Figures 2a, 2d and 2f, 2i).

3.3. Ventilation Patterns and Global Circulation

Ventilation of the global ocean in our simulations is forced by deep water formation in the southern Pacific Ocean (Figure 3a), as simulated for late Cretaceous configurations in previous studies (e.g., Ladant et al., 2020; Laugié et al., 2021; Monteiro et al., 2012). Highly oxygenated waters spread in the deep Pacific basin and then recirculate through the Tethys and northern Pacific Oceans before eventually reaching the Atlantic Ocean through the Central American Seaway, gradually losing oxygen along their journey (Laugié et al., 2021). Already strongly O_2-depleted Pacific Ocean deep waters (>2,500 m) therefore feed the Central Atlantic basin (Laugié et al., 2021), which is the most sensitive basin to oxygen depletion in our orbital set of simulations (Figure 1b). The northward limit of highly oxygenated waters (>200 mmol/m^3 isoline on Figure S7 in Supporting Information S1) in the southern deep Pacific Ocean is reduced in HOSP (40°S) compared to HO (15°S) because the overturning circulation is overall slower (up to 4 Sv decrease) when eccentricity is high (HOSP) (Figure 3b). Overall, the strength of deoxygenation at the global scale (Figure 1b) between the simulations scales with the change in intensity of the Meridional Overturning Circulation (Figure 3b and Figure S9 in Supporting Information S1).

The change in overturning circulation in HOSP is induced by less intense deep convection in the high latitudes of the southern Pacific under high eccentricity (Figures 3a and 3c and Figure S10 in Supporting Information S1). The slower rate of deep water formation is promoted by a shallower mixed layer along the western Antarctica margin during the late austral winter that only reach a maximum depth of 2,500 m in HOSP compared to 3,500 m in HO (in which the mixed layer is the deepest) (Figure 3c). Reduced convection at sites of deep water formation is coherent with the local increase in the surface moisture balance (P-E budget) that translates into a decrease in

surface salinity in HOSP (Figure S8 in Supporting Information S1). A similar pattern is depicted in other high eccentricity simulations (Figure S10 in Supporting Information S1).

4. Discussion

4.1. Basin-Scale Orbital Heartbeats of Anoxia

Our simulations show that orbitally induced changes in deep ocean ventilation can generate strong variations in the expansion of anoxia at the scale of the Atlantic basin. Overall, the imprint of this ventilation effect depends on the background oxygenation state of water masses: perceptible changes in oxygenation state would be expected in basins that are already strongly depleted in oxygen or close to a threshold such as the Cenomano-Turonian proto-Atlantic basin. This suggest that isolated oceanic basins are more likely to become periodically anoxic and that trends simulated for the Atlantic basin would likely be applicable at smaller scales, in complex paleogeography settings that are not well represented at the resolution of our model (e.g., western Neotethys, Golonka et al. (2000)). Our results suggest in addition that sensitivity to orbital variations of a specific basin could therefore evolved over time with the tectonic forcing, as could be the case for instance for the southern Atlantic Ocean (Dummann et al., 2021), which became progressively less isolated from the global ocean during the late Cretaceous and therefore likely less prone to periodic deoxygenation.

The simulated deep ocean ventilation is strongly sensitive to both eccentricity and precession forcing and to a lower extent to obliquity. The latter result suggest that ephemeral high latitude ice-sheets is not a requirement to drive obliquity-scale variations in hot-house oceans and support Meyers et al. (2012) hypothesis which considers periodic expansions of anoxia in the northern Atlantic basin as the result of orbitally driven ventilation cycles transmitted from mid-to low-latitudes of the Central Atlantic basin. Yet, in our simulations, the signal does not arise from the northern Atlantic Ocean but from the southern Pacific Ocean where deep waters form in our Cenomanian-Turonian paleogeographic configurations. Eccentricity driven change in ventilation that we simulated in this study are consistent with Lunt et al. (2011) who also simulated deep ocean circulation changes driven by eccentricity in Paleocene simulations, under high CO_2 concentration. Here in addition, we show that such changes in ocean circulation influence the oxygenation state of the ocean. The strong deoxygenation induced by ventilation at eccentricity and precession frequencies highlight that cyclicity with such signature in OM deposits are not purely controlled by tropical processes as usually admitted (e.g., Wagner et al., 2013).

4.2. Implications for Anoxia Expansion During OAEs

In this study, we highlight that the occurrence of cyclic changes in oxygenation state at basin scale depends on the global ocean oxygenation background. The ventilation process we describe here—although being only simulated in the Atlantic basins in the configurations we used—might therefore extend to other restricted basins and help explaining changes in orbital signature of OAEs sediments (e.g., Meyers et al., 2012). During OAEs, the global ocean is indeed less oxygenated due to increasing biological activity forced by nutrient released both related to enhanced hydrological cycle and volcanic activity (e.g., Du Vivier et al., 2014; Kuroda et al., 2007; Turgeon & Creaser, 2008). Increased deoxygenation could force basins whose oxygenation state was close to dysoxia/anoxia prior to the OAE across a threshold. This would result in appearance of orbitally driven cyclicity, whereas those basins would have been previously hampered from ventilation-driven change in background oxygenation before the OAE. It could be the case for the deep European Tethys platform in our simulations, as the basin has intermediate O_2 concentration and is close to the oxygenation threshold for dysoxia (Figure 1a). This effect would be enhanced due to phasing of OAEs event with high eccentricity period as being suggested from cyclostratigraphic studies on Bonarelli and Livio sections (Umbria-Marche Basin; Batenburg et al. (2016)) and Tarfaya shelf (Morroco; Kuhnt et al. (2017)) that both placed the beginning of OAE2 in their records at the first eccentricity maxima following a long-term eccentricity minima (2.4 Myr eccentricity cycle). Both decreasing global water masses oxygenation during OAEs and phasing of the event with increasing eccentricity could for example, partially explain why the western Neotethys area became more prone to precession-modulated cyclic anoxia during the OAE2 such as suggested by Batenburg et al. (2016) based on increased black cherts occurrence. The phenomena described above would also superimposed with the change of ocean ventilation sensitivity to orbital configuration varying with pCO_2 (Dummann et al., 2021) and radiative forcing (Lunt et al., 2011)

suggesting that the effect of eccentricity-driven global deoxygenation would be mechanically amplified during extreme greenhouse episodes.

4.3. Limitations and Future Directions

The present study enables us to shed light on one of the mechanisms by which orbital parameters might have affected the global climate system and the sedimentary records of greenhouse climate periods and helps to improve the understanding of cyclicity recorded in the Cretaceous sediments. The ventilation process described here for the first time should be considered a "background" signal and might interact with other processes. Orbitally driven changes in continental hydrology and weathering, as well as subsequent modifications in freshwater discharge and nutrient delivery, driving increases in biological activity is in general the most favored hypothesis to explain OM cyclicity in sedimentary sequences (e.g., Beckmann et al., 2005; Charbonnier et al., 2018; Flögel et al., 2008; van Helmond et al., 2015; Wagner et al., 2013). Evaluating the relative influence of this chain of processes versus deep ocean ventilation would require more in-depth regional to local analyzes as well as the inclusion of additional processes that are not represented in the model we used. For example, in some sedimentary basins, such as the Deep Ivory basin in the Equatorial Atlantic region, the continental hydrology dynamics and freshwater discharge probably matter more than oceanic processes in controlling the OM deposition (Beckmann et al., 2005; Flögel et al., 2008). In addition, terrestrial OM can contribute to carbon accumulation in some sedimentary basins (Wagner et al., 2013) but this process has been ignored in our study. Including nutrient fluxes backed by a realistic estimation of hinterland weathering as well as taking into account fluxes of terrestrial OM would be of great help to better understand the cyclicity in OM deposits at a more local scale. Ultimately, in regions where ocean productivity is strongly reliant on dust fertilization, the export of carbon to the abyss could vary with changes in hinterland aridity as well as winds pattern. We have deliberately left aside all these local processes because we wanted to emphasize the overlooked role of orbitally induced changes in global ocean dynamics and its consequences on the ocean oxygenation state.

Data Availability Statement

Code availability LMDZ, XIOS, NEMO, and ORCHIDEE are released under the terms of the CeCILL license. OASIS-MCT is released under the terms of the Lesser GNU General Public License (LGPL). Up to date IPSL-CM5A2 source code is publicly available through svn, with the following commands line: svn co http://forge.ipsl.jussieu.fr/igcmg/svn/modipsl/branches/publications/IPSLCM5A2.1_11192019%20modipsl;%20cd%20modipsl/util;./model%20IPSLCM5A2.1. The mod.def file provides information regarding the different revisions used, namely:

- NEMOGCM branch nemo_v3_6_STABLE revision 6665
- XIOS2 branchs/xios-2.5 revision 1763
- IOIPSL/src svn tags/v2_2_2
- LMDZ5 branches/IPSLCM5A2.1 rev 3591
- branches/publications/ORCHIDEE_IPSLCM5A2.1.r5307 rev 6336
- OASIS3-MCT 2.0_branch (rev 4775 IPSL server). The login/password combination requested at first use to download the ORCHIDEE component is anonymous/anonymous.

We recommend that you refer to the project website: http://forge.ipsl.jussieu.fr/igcmg_doc/wiki/Doc/Config/IPSLCM5A2 for a proper installation and compilation of the environment. In addition, source code of the version used for this paper is publicly available at https://doi.org/10.5281/zenodo.6772699 (Pillot, 2022). The authors acknowledge the use of Generic Mapping Tool (generic-mapping-tools.org, Wessel et al. (2013)), pyferret (ferret.pmel.noaa.gov/Ferret/) and NCL (https://www.ncl.ucar.edu) for analysis and graphics. Colored figures in this paper were made with perceptually uniform, color-vision-deficiency-friendly scientific color maps (Crameri et al., 2020), developed and distributed by Fabio Crameri (https://www.fabiocrameri.ch/colourmaps/). All model outputs used in this study are available as a NetCDF files on a Zenodo repository and accessible at https://doi.org/10.5281/zenodo.6641306 (Sarr & Laugié, 2022). The repository also contains paleogeography grids used for the simulations.

Acknowledgments
The authors acknowledge Olivier Aumont, Christian Ethé and Laurent Bopp for their contribution to the development of the adapted version of the PISCES code for deep-time simulations. The authors thank the CEA/CCRT for providing access to the HPC resources of TGCC under the allocation 2019-A0050102212, 2020-A0090102212 and 2021-A0110102212 made by GENCI. The authors thank TotalEnergies for funding the project and granting permission to publish. The authors are also grateful to David de Vleeschouwer and Michel Crucifix for their comments and reviews.

References

Aumont, O., Éthé, C., Tagliabue, A., Bopp, L., & Gehlen, M. (2015). PISCES-v2: An ocean biogeochemical model for carbon and ecosystem studies. *Geoscientific Model Development*, *8*(8), 2465–2513. https://doi.org/10.5194/gmd-8-2465-2015

Barron, E. J., Arthur, M. A., & Kauffman, E. G. (1985). Cretaceous rhythmic bedding sequences: A plausible link between orbital variations and climate. *Earth and Planetary Science Letters*, *72*(4), 327–340. https://doi.org/10.1016/0012-821x(85)90056-1

Batenburg, S. J., De Vleeschouwer, D., Sprovieri, M., Hilgen, F. J., Gale, A. S., Singer, B. S., et al. (2016). Orbital control on the timing of oceanic anoxia in the late cretaceous. *Climate of the Past*, *12*(10), 1995–2009. https://doi.org/10.5194/cp-12-1995-2016

Beckmann, B., Flögel, S., Hofmann, P., Schulz, M., & Wagner, T. (2005). Orbital forcing of Cretaceous river discharge in tropical Africa and ocean response. *Nature*, *437*(7056), 241–244. https://doi.org/10.1038/nature03976

Behrooz, L., Naafs, B., Dickson, A., Love, G., Batenburg, S., & Pancost, R. (2018). Astronomically driven variations in depositional environments in the south Atlantic during the early cretaceous. *Paleoceanography and Paleoclimatology*, *33*(8), 894–912. https://doi.org/10.1029/2018pa003338

Beil, S., Kuhnt, W., Holbourn, A. E., Aquit, M., Flögel, S., Chellai, E. H., & Jabour, H. (2018). New insights into Cenomanian paleoceanography and climate evolution from the Tarfaya basin, southern Morocco. *Cretaceous Research*, *84*, 451–473. https://doi.org/10.1016/j.cretres.2017.11.006

Bopp, L., Resplandy, L., Untersee, A., Le Mezo, P., & Kageyama, M. (2017). Ocean (de) oxygenation from the last glacial maximum to the twenty-first century: Insights from Earth system models. *Philosophical Transactions of the Royal Society A: Mathematical, Physical & Engineering Sciences*, *375*(2102), 20160323. https://doi.org/10.1098/rsta.2016.0323

Charbonnier, G., Boulila, S., Spangenberg, J. E., Adatte, T., Föllmi, K. B., & Laskar, J. (2018). Obliquity pacing of the hydrological cycle during the Oceanic Anoxic Event 2. *Earth and Planetary Science Letters*, *499*, 266–277. https://doi.org/10.1016/j.epsl.2018.07.029

Crameri, F., Shephard, G. E., & Heron, P. J. (2020). The misuse of colour in science communication. *Nature Communications*, *11*(1), 1–10. https://doi.org/10.1038/s41467-020-19160-7

Dickson, A. J., Saker-Clark, M., Jenkyns, H. C., Bottini, C., Erba, E., Russo, F., et al. (2017). A southern hemisphere record of global trace-metal drawdown and orbital modulation of organic-matter burial across the Cenomanian–Turonian boundary (ocean drilling program site 1138, Kerguelen Plateau). *Sedimentology*, *64*(1), 186–203. https://doi.org/10.1111/sed.12303

Dummann, W., Steinig, S., Hofmann, P., Lenz, M., Kusch, S., Flögel, S., et al. (2021). Driving mechanisms of organic carbon burial in the early cretaceous south Atlantic cape basin (dsdp site 361). *Climate of the Past*, *17*(1), 469–490. https://doi.org/10.5194/cp-17-469-2021

Du Vivier, A. D., Selby, D., Sageman, B. B., Jarvis, I., Gröcke, D. R., & Voigt, S. (2014). Marine 187os/188os isotope stratigraphy reveals the interaction of volcanism and ocean circulation during oceanic anoxic event 2. *Earth and Planetary Science Letters*, *389*, 23–33. https://doi.org/10.1016/j.epsl.2013.12.024

Einsele, G. (1982). *Cyclic and event stratification*. Springer-Verlag.

Eldrett, J. S., Ma, C., Bergman, S. C., Lutz, B., Gregory, F. J., Dodsworth, P., et al. (2015). An astronomically calibrated stratigraphy of the Cenomanian, Turonian and earliest Coniacian from the cretaceous western interior seaway, USA: Implications for global chronostratigraphy. *Cretaceous Research*, *56*, 316–344. https://doi.org/10.1016/j.cretres.2015.04.010

Erb, M. P., Broccoli, A. J., Graham, N. T., Clement, A. C., Wittenberg, A. T., & Vecchi, G. A. (2015). Response of the equatorial Pacific seasonal cycle to orbital forcing. *Journal of Climate*, *28*(23), 9258–9276. https://doi.org/10.1175/jcli-d-15-0242.1

Floegel, S., & Wagner, T. (2006). Insolation-control on the late cretaceous hydrological cycle and tropical African climate—Global climate modelling linked to marine climate records. *Palaeogeography, Palaeoclimatology, Palaeoecology*, *235*(1–3), 288–304. https://doi.org/10.1016/j.palaeo.2005.09.034

Flögel, S., Beckmann, B., Hofmann, P., Bornemann, A., Westerhold, T., Norris, R. D., et al. (2008). Evolution of tropical watersheds and continental hydrology during the late Cretaceous greenhouse; impact on marine carbon burial and possible implications for the future. *Earth and Planetary Science Letters*, *274*(1–2), 1–13. https://doi.org/10.1016/j.epsl.2008.06.011

Golonka, J., Oszczypko, N., & Ślączka, A. (2000). Late carboniferous-neogene geodynamic evolution and paleogeography of the circum-Carpathian region and adjacent areas. In *Annales societatis geologorum poloniae* (Vol. *70*, pp. 107–136).

Herbert, T. D., & Fischer, A. G. (1986). Milankovitch climatic origin of mid-cretaceous black shale rhythms in central Italy. *Nature*, *321*(6072), 739–743. https://doi.org/10.1038/321739a0

Hofmann, P., & Wagner, T. (2011). ITCZ controls on late cretaceous black shale sedimentation in the tropical Atlantic ocean. *Paleoceanography*, *26*(4), 2011PA002154. https://doi.org/10.1029/2011pa002154

Kolonic, S., Wagner, T., Forster, A., Sinninghe Damsté, J. S., Walsworth-Bell, B., Erba, E., et al. (2005). Black shale deposition on the northwest African shelf during the Cenomanian/Turonian oceanic anoxic event: Climate coupling and global organic carbon burial. *Paleoceanography*, *20*(1). https://doi.org/10.1029/2003pa000950

Kuhnt, W., Holbourn, A. E., Beil, S., Aquit, M., Krawczyk, T., Flögel, S., et al. (2017). Unraveling the onset of cretaceous Oceanic Anoxic Event 2 in an extended sediment archive from the Tarfaya-Laayoune basin, Morocco. *Paleoceanography*, *32*(8), 923–946. https://doi.org/10.1002/2017pa003146

Kuroda, J., Ogawa, N. O., Tanimizu, M., Coffin, M. F., Tokuyama, H., Kitazato, H., & Ohkouchi, N. (2007). Contemporaneous massive subaerial volcanism and late Cretaceous Oceanic Anoxic Event 2. *Earth and Planetary Science Letters*, *256*(1–2), 211–223. https://doi.org/10.1016/j.epsl.2007.01.027

Kuypers, M. M., Lourens, L. J., Rijpstra, W. I. C., Pancost, R. D., Nijenhuis, I. A., & Damsté, J. S. S. (2004). Orbital forcing of organic carbon burial in the proto-north Atlantic during Oceanic Anoxic Event 2. *Earth and Planetary Science Letters*, *228*(3–4), 465–482. https://doi.org/10.1016/j.epsl.2004.09.037

Ladant, J.-B., Poulsen, C. J., Fluteau, F., Tabor, C. R., MacLeod, K. G., Martin, E. E., et al. (2020). Paleogeographic controls on the evolution of late Cretaceous ocean circulation. *Climate of the Past*, *16*(3), 973–1006. https://doi.org/10.5194/cp-16-973-2020

Laskar, J., Fienga, A., Gastineau, M., & Manche, H. (2011). La2010: A new orbital solution for the long-term motion of the Earth. *Astronomy & Astrophysics*, *532*, A89. https://doi.org/10.1051/0004-6361/201116836

Laskar, J., Robutel, P., Joutel, F., Gastineau, M., Correia, A., & Levrard, B. (2004). A long-term numerical solution for the insolation quantities of the Earth. *Astronomy & Astrophysics*, *428*(1), 261–285. https://doi.org/10.1051/0004-6361:20041335

Laugié, M., Donnadieu, Y., Ladant, J.-B., Bopp, L., Ethé, C., & Raisson, F. (2021). Exploring the impact of Cenomanian paleogeography and marine gateways on oceanic oxygen. *Paleoceanography and Paleoclimatology*, *36*(7), e2020PA004202. https://doi.org/10.1029/2020pa004202

Laugié, M., Donnadieu, Y., Ladant, J.-B., Green, J., Bopp, L., & Raisson, F. (2020). Stripping back the modern to reveal the Cenomanian–Turonian climate and temperature gradient underneath. *Climate of the Past*, *16*(3), 953–971. https://doi.org/10.5194/cp-16-953-2020

Li, Y.-X., Gill, B., Montañez, I. P., Ma, L., LeRoy, M., & Kodama, K. P. (2020). Orbitally driven redox fluctuations during Cretaceous Oceanic Anoxic Event 2 (OAE2) revealed by a new magnetic proxy. *Palaeogeography, Palaeoclimatology, Palaeoecology*, *538*, 109465. https://doi.org/10.1016/j.palaeo.2019.109465

Lunt, D. J., Ridgwell, A., Sluijs, A., Zachos, J., Hunter, S., & Haywood, A. (2011). A model for orbital pacing of methane hydrate destabilization during the Palaeogene. *Nature Geoscience*, *4*(11), 775–778. https://doi.org/10.1038/ngeo1266

Meyers, S. R., Sageman, B. B., & Arthur, M. A. (2012). Obliquity forcing of organic matter accumulation during Oceanic Anoxic Event 2. *Paleoceanography*, *27*(3). https://doi.org/10.1029/2012pa002286

Middelburg, J., & Levin, L. (2009). Coastal hypoxia and sediment biogeochemistry. *Biogeosciences*, *6*(7), 1273–1293. https://doi.org/10.5194/bg-6-1273-2009

Mitchell, R. N., Bice, D. M., Montanari, A., Cleaveland, L. C., Christianson, K. T., Coccioni, R., & Hinnov, L. A. (2008). Oceanic anoxic cycles? Orbital prelude to the Bonarelli level (OAE 2). *Earth and Planetary Science Letters*, *267*(1–2), 1–16. https://doi.org/10.1016/j.epsl.2007.11.026

Monteiro, F. M., Pancost, R. D., Ridgwell, A., & Donnadieu, Y. (2012). Nutrients as the dominant control on the spread of anoxia and euxinia across the Cenomanian-Turonian Oceanic Anoxic Event (OAE2): Model-data comparison. *Paleoceanography*, *27*(4). https://doi.org/10.1029/2012pa002351

Müller, R. D., Sdrolias, M., Gaina, C., & Roest, W. R. (2008). Age, spreading rates, and spreading asymmetry of the world's ocean crust. *Geochemistry, Geophysics, Geosystems*, *9*(4). https://doi.org/10.1029/2007gc001743

Park, J., & Oglesby, R. J. (1991). Milankovitch rhythms in the cretaceous: A GCM modelling study. *Global and Planetary Change*, *4*(4), 329–355. https://doi.org/10.1016/s0031-0182(12)80034-4

Pillot, Q. (2022). IPSL-CM5A2 source code used for "evolution of ocean circulation in the north atlantic ocean during the miocene: Impact of the Greenland ice sheet and the eastern tethys seaway. [software]. Zenodo. https://doi.org/10.5281/zenodo.6772699.

Rossignol-Strick, M. (1985). Mediterranean quaternary sapropels, an immediate response of the african monsoon to variation of insolation. *Palaeogeography, Palaeoclimatology, Palaeoecology*, *49*(3–4), 237–263. https://doi.org/10.1016/0031-0182(85)90056-2

Sageman, B. B., Rich, J., Arthur, M. A., Birchfield, G., & Dean, W. (1997). Evidence for milankovitch periodicities in Cenomanian-Turonian lithologic and geochemical cycles, western interior USA. *Journal of Sedimentary Research*, *67*(2), 286–302.

Sarr, A.-C., & Laugié, M. (2022). Late cretaceous (Cenomanian-Turonian) ocean deoxygenation variability in response to idealized orbital configurations. [dataset]. Zenodo. https://doi.org/10.5281/zenodo.6641306.

Sepulchre, P., Caubel, A., Ladant, J.-B., Bopp, L., Boucher, O., Braconnot, P., et al. (2020). IPSL-CM5A2–an Earth system model designed for multi-millennial climate simulations. *Geoscientific Model Development*, *13*(7), 3011–3053. https://doi.org/10.5194/gmd-13-3011-2020

Sewall, J. V., Van De Wal, R., Van Der Zwan, K., Van Oosterhout, C., Dijkstra, H., & Scotese, C. (2007). Climate model boundary conditions for four Cretaceous time slices. *Climate of the Past*, *3*(4), 647–657. https://doi.org/10.5194/cp-3-647-2007

Sloan, L. C., & Huber, M. (2001). Eocene oceanic responses to orbital forcing on precessional time scales. *Paleoceanography*, *16*(1), 101–111. https://doi.org/10.1029/1999pa000491

Turgeon, S. C., & Creaser, R. A. (2008). Cretaceous Oceanic Anoxic Event 2 triggered by a massive magmatic episode. *Nature*, *454*(7202), 323–326. https://doi.org/10.1038/nature07076

Tyson, R. V., & Pearson, T. H. (1991). Modern and ancient continental shelf anoxia: An overview. *Geological Society, London, Special Publications*, *58*(1), 1–24. https://doi.org/10.1144/gsl.sp.1991.058.01.01

van Helmond, N. A., Sluijs, A., Sinninghe Damsté, J., Reichart, G.-J., Voigt, S., Erbacher, J., et al. (2015). Freshwater discharge controlled deposition of Cenomanian–Turonian black shales on the NW European epicontinental shelf (Wunstorf, northern Germany). *Climate of the Past*, *11*(3), 495–508. https://doi.org/10.5194/cp-11-495-2015

Voigt, S., Erbacher, J., Mutterlose, J., Weiss, W., Westerhold, T., Wiese, F., et al. (2008). The Cenomanian-Turonian of the Wunstorf section-(north Germany): Global stratigraphic reference section and new orbital time scale for Oceanic Anoxic Event 2. *Newsletters in Stratigraphy*, *43*(1), 65–89. https://doi.org/10.1127/0078-0421/2008/0043-0065

Wagner, T., Hofmann, P., & Flögel, S. (2013). Marine black shale deposition and hadley cell dynamics: A conceptual framework for the Cretaceous Atlantic ocean. *Marine and Petroleum Geology*, *43*, 222–238. https://doi.org/10.1016/j.marpetgeo.2013.02.005

Wang, Y., Bodin, S., Blusztajn, J. S., Ullmann, C., & Nielsen, S. G. (2022). Orbitally paced global oceanic deoxygenation decoupled from volcanic CO_2 emission during the middle Cretaceous Oceanic Anoxic Event 1b (Aptian-Albian transition). *Geology*. https://doi.org/10.1130/g50553.1

Wessel, P., Smith, W. H., Scharroo, R., Luis, J., & Wobbe, F. (2013). Generic mapping tools: Improved version released. *Eos, Transactions American Geophysical Union*, *94*(45), 409–410. https://doi.org/10.1002/2013eo450001

Westerhold, T., Marwan, N., Drury, A. J., Liebrand, D., Agnini, C., Anagnostou, E., et al. (2020). An astronomically dated record of Earth's climate and its predictability over the last 66 million years. *Science*, *369*(6509), 1383–1387. https://doi.org/10.1126/science.aba6853

Winguth, A., & Winguth, C. (2013). Precession-driven monsoon variability at the permian–triassic boundary—Implications for anoxia and the mass extinction. *Global and Planetary Change*, *105*, 160–170. https://doi.org/10.1016/j.gloplacha.2012.06.006